Arginase 1 is an innate lymphoid cell-intrinsic metabolic checkpoint controlling type 2 inflammation

Laurel A Monticelli[1], **Michael D Buck**[2], **Anne-Laure Flamar**[1], **Steven A Saenz**[1,6], **Elia D Tait Wojno**[1,6], **Naomi A Yudanin**[1], **Lisa C Osborne**[1,6], **Matthew R Hepworth**[1], **Sara V Tran**[1], **Hans-Reimer Rodewald**[3], **Hardik Shah**[4], **Justin R Cross**[4], **Joshua M Diamond**[5], **Edward Cantu**[5], **Jason D Christie**[5], **Erika L Pearce**[2], and **David Artis**[1]

[1]Jill Roberts Institute for Research in Inflammatory Bowel Disease, Joan and Sanford I. Weill Department of Medicine, Department of Microbiology and Immunology, Weill Cornell Medicine, Cornell University, New York, NY USA

[2]Department of Immunometabolism, Max Plank Institute of Immunobiology and Epigenetics, Freiburg, Germany

[3]Division of Cellular Immunology, German Cancer Research Center (DKFZ), Heidelberg, Germany

[4]Donald B. and Catherine C. Marron Cancer Metabolism Center, Memorial Sloan Kettering Cancer Center, New York, NY USA

[5]Division of Cardiovascular Surgery, Center for Translational Lung Biology, University of Pennsylvania, Perelman School of Medicine, Philadelphia, PA USA

Abstract

Group 2 innate lymphoid cells (ILC2s) regulate tissue inflammation and repair following activation by cell-extrinsic factors including host-derived cytokines. However, the cell-intrinsic metabolic pathways that control ILC2 function are undefined. Here we demonstrate that expression of the enzyme Arginase 1 (Arg1) is a conserved trait of murine and human ILC2s during acute or chronic lung inflammation. Deletion of murine ILC-intrinsic Arg1 abrogated type 2 lung inflammation by restraining ILC2 proliferation and dampening cytokine production. Mechanistically, inhibition of Arg1 enzymatic activity disrupted multiple components of ILC2

Corresponding author: David Artis, PhD, Weill Cornell Medicine, Cornell University, Belfer Research Building, room 702 (box 190), 413 East 69th Street, New York, NY 10021. USA, ; Email: dartis@med.cornell.edu
[6]Present addresses: Biogen, Inc., Cambridge, MA USA (S.A.S), Baker Institute for Animal Health, Department of Microbiology and Immunology, Cornell University College of Veterinary Medicine, Ithaca, NY USA (E.D.T.W), Department of Microbiology & Immunology, University of British Columbia, Vancouver BC Canada (L.C.O)

metabolic programming by altering arginine catabolism, impairing polyamine biosynthesis and reducing aerobic glycolysis. These data identify Arg1 as a key regulator of ILC2 bioenergetics, controlling proliferative capacity and pro-inflammatory functions that promote type 2 inflammation.

The innate lymphoid cell (ILC) family orchestrates immunity, inflammation, metabolic homeostasis and tissue repair in multiple tissues including the intestine, liver, adipose, skin and lung[1,2]. Group 2 ILCs (ILC2s) are the dominant ILC population in the human and murine lung where they act as key initiators of allergen and non-allergen-induced type 2 inflammation[1,3–5] as well as promoting airway tissue repair[6]. ILC2s are activated by cell-extrinsic environmental cues including the cytokines interleukin-25 (IL-25), IL-33 and thymic stromal lymphopioetin (TSLP)[1,2]. However, the cell-intrinsic pathways that regulate ILC2 effector function remain poorly characterized. In particular, regulation of cell metabolism is a critical determinant of adaptive lymphocyte development and function[7,8], although whether cell-intrinsic metabolic signals influence ILC biology is unknown. The enzyme Arginase 1 (Arg1) was identified as a marker of ILC fetal intestinal precursors and adult lung ILC2s[9,10], although the functional significance of Arg1 enzymatic activity in ILCs remains unclear.

Arg1 metabolizes the amino acid L-arginine to generate urea and ornithine, whose downstream metabolites proline and polyamines drive collagen synthesis and bioenergetic pathways critical for cell proliferation[11–13]. Although homeostatic L-arginine metabolism occurs primarily in the liver to complete the urea cycle, immune cells can serve as critical extra-hepatic sites of Arg1 activity during infection and tissue inflammation[12–16]. Particularly in the context of cancer or type 2 cytokine-driven inflammation in the intestine, liver and skin, Arg1 activity is a key signature of alternatively activated macrophages (AAMacs)[15,16]. AAMac-derived Arg1 primarily acts extrinsically, promoting wound healing and tissue fibrosis through eliciting collagen synthesis by fibroblasts or by limiting T cell responses via nutrient deprivation of L-arginine[14,17–19]. In contrast, in the lung, evidence supporting the functional significance of AAMac-derived Arg1 enzymatic activity remains controversial. For example, models targeting macrophage-specific Arg1 have failed to recapitulate the effects observed in studies using global inhibition of Arg1 to dampen airway inflammation[19–23], suggesting that other cell populations may be responsible for the ability of Arg1 to promote development of lung disease. We demonstrate here that Arg1 has a critical cell-intrinsic role in regulating ILC2 metabolism and the development of type 2 inflammation.

Results

Constitutive Arg1 expression in precursor and mature ILC2

Arg1 expression has been reported in a population of ILC precursors in the fetal intestine and in mature ILC2s in the lung[9,10]. Whether Arg1 is differentially expressed in distinct adult ILC precursors or mature ILC populations and how this is influenced by the tissue microenvironment remains poorly characterized. Examination of bone marrow hematopoietic stem cells (HSCs), common lymphoid progenitors (CLPs) and the common

innate lymphoid progenitor (CHILP) in reporter mice that express yellow fluorescent protein under control of the Arg1 promoter ($Arg1^{YFP}$) did not reveal any expression of Arg1-YFP (Fig. 1a), suggesting that upregulation of Arg1 in the adult bone marrow occurs at a later developmental checkpoint during subset differentiation of the ILC lineages. Consistent with this, analysis of Arg1-YFP expression in lineage-specified ILC2 bone marrow precursors that lack KLRG1 (termed 'ILC2Ps')[24] revealed high expression of Arg1-YFP equivalent to that observed in mature KLRG1^{+} ILC2s (Fig. 1b). Taken together, these data identify Arg1 as a marker of ILC2 lineage-committed precursors in the adult bone marrow.

To investigate whether Arg1 expression in mature ILC2s is influenced by their distinct tissue microenvironment, we examined Arg1 expression in ILC2s isolated from multiple lymphoid, mucosal and adipose tissues. ILC2s in the lung expressed high amounts of Arg1 protein, as measured both by intracellular staining and by expression of Arg1-YFP (Fig. 1c). Further flow cytometric profiling of mature KLRG1^{+} ILC2s isolated from multiple tissues of $Arg1^{YFP}$ mice including spleen (SPL), mesenteric lymph node (mLN), small intestine (SI), large intestine (LI) and epididymal white adipose tissue (EWAT) (Fig. 1d) revealed that constitutive Arg1 expression represents a conserved trait of mature ILC2s across lymphoid and non-lymphoid tissues.

Murine ILC2s express Arg1 in the inflamed lung

In contrast to lymphoid tissues and barrier surfaces such as the intestine that contain all three subsets of ILCs, the murine lung is dominated by ILC2s[3,6]. Given the role of Arg1 in regulating lung homeostasis in the context of infection and inflammation[15,16,25,26], we sought to examine which cell populations are the dominant sources of Arg1. Unbiased flow cytometric analysis of total Arg1-YFP-expressing cells in lungs of naive $Arg1^{YFP}$ mice revealed that the majority of Arg1 was expressed by lineage negative (Lin^{−}) cells that expressed CD90, CD25, CD127 and IL-33R, identifying them as ILC2s (Fig. 1e,f). Comprehensive examination of multiple innate and adaptive immune cell lineages in the lungs of $Arg1^{YFP}$ mice confirmed that ILC2s are the dominant cellular source of Arg1 under homeostatic conditions (Fig. 1g).

ILC2s can promote type 2 inflammation in the lung in response to a variety of allergic and non-allergic stimuli[1,2], although the cell-intrinsic factors regulating their pro-inflammatory functions remain poorly characterized. To investigate whether ILC2-intrinsic Arg1 influences lung inflammation, we employed a murine model of acute allergen-induced airway inflammation. Intranasal instillation of papain into $Arg1^{YFP}$ mice resulted in elevated $Arg1$ mRNA expression in the lung compared to PBS-treated controls (Fig. 2a), correlating with increased frequencies of ILC2s in the lung parenchyma (Fig. 2b). These ILC2s retained high expression of Arg1-YFP following allergen exposure (Fig. 2c), resulting in elevated frequencies and total cell numbers of Arg1-expressing ILC2s compared to PBS-treated control mice (Fig. 2d,e). Further, unbiased analysis of total Arg1-YFP^{+} cells revealed that ILC2s constituted a major source of Arg1 expression in the inflamed lung (Fig. 2f,g). These data suggest that ILC-intrinsic expression of Arg1 influences development or progression of lung inflammation.

Human ILC2s express Arg1 during lung disease

Elevated expression of Arg1 and dysregulation of arginine metabolism has been reported in patients diagnosed with asthma[25–28] as well as chronic obstructive pulmonary disease (COPD)[29,30] and idiopathic pulmonary fibrosis (IPF)[17]. However, the cellular sources of this enzyme in human lung disease are incompletely understood and presumed to be limited to the myeloid lineage[11,12,31]. Using primary lung tissue obtained from patients diagnosed with COPD or IPF, we next sought to test whether Arg1 is expressed by ILCs during human inflammatory lung disease. Flow cytometric analysis of lineage negative Lin⁻CD127⁺ ILCs identified all ILC1, ILC2 and ILC3 populations in human explant tissues (Fig. 3a) although total ILC frequency and subset distribution did not appear to differ significantly between disease states (Supplementary Fig. 1a,b). However, examination of intracellular Arg1 expression revealed a pattern of differential expression among ILC subsets in which IL-33R⁺ ILC2s expressed Arg1 and this expression was comparable with CD14⁺CD16⁺ myeloid cells (Fig. 3b,c). Within ILC2s, Arg1 expression did not differ significantly between patients diagnosed with COPD versus IPF (Supplementary Fig. 1c), suggesting that Arg1 expression may be a more generalized signature of these innate cells during inflammatory conditions and could represent a novel target for clinical therapies modulating arginine metabolism.

Deletion of ILC-intrinsic Arg1 dampens airway inflammation

To investigate the role of ILC2-derived Arg1, we generated a genetic mouse model that deletes Arg1 in ILCs using a cre recombinase targeting cells expressing the IL-7Rα chain (*Il7r*$^{Cre/+}$). Fate-mapping analysis using *Il7r*$^{Cre/+}$ mice crossed to *Rosa26*$^{floxSTOP-eYFP}$ mice revealed that all lung ILC2s were marked with a history of IL-7Rα expression (Fig. 4a). Notably, although CD4⁺ T cells, B cells and NK cells were also marked by a history of IL-7Rα expression (Supplementary Fig. 2), none of these cells expressed Arg1-YFP under steady-state conditions or during papain-induced lung inflammation (Supplementary Fig. 3). Therefore, use of the IL-7Rα cre recombinase in combination with Arg1 flox/flox mice generates a mouse that lacks Arg1 specifically in ILCs (called *Arg1*^{ILC} here). Transcriptional (Fig. 4b) and flow cytometric (Fig. 4c) analysis confirmed efficient deletion of Arg1 expression in lung ILC2s.

To test whether ILC-intrinsic Arg1 plays a role in the development of lung inflammation, we treated *Arg1*$^{fl/fl}$, *Arg1*$^{+/+}$*Il7r*$^{Cre/+}$ controls and *Arg1*^{ILC} mice with PBS or papain and assessed for immunologic and pathologic parameters of type 2 lung inflammation. All groups treated with control PBS had equivalent frequencies of lung ILC2s (Fig. 4d,e), suggesting that despite constitutive expression of Arg1, this enzyme was not required for the development, maturation or maintenance of ILC2s. While exposure to papain resulted in increased frequencies (Fig. 4d,e) and total cell numbers (Fig. 4f) of ILC2s in the lungs of *Arg1*$^{fl/fl}$ and *Arg1*$^{+/+}$*Il7r*$^{Cre/+}$ mice, loss of ILC-intrinsic Arg1 expression severely diminished papain-induced ILC2 responses in *Arg1*^{ILC} mice (Fig. 4d–f). The failure to mount an ILC2 response correlated with decreased *Arg1* expression in lung homogenates of *Arg1*^{ILC} (Fig. 4g), consistent with ILC2s being a critical regulator of Arg1 in the inflamed lung.

ILC2s are the primary source of the type 2 cytokines IL-5 and IL-13 during acute papain-induced inflammation and these cytokines are critical for driving eosinophilia and the T_H2 subset of CD4^{+} T cell responses, respectively[4,5]. Correlating with the reduction in ILC2 cell numbers, expression of *Il5* (Fig. 4h) and *Il13* (Fig. 4i) in lung homogenates was significantly reduced in papain-treated *Arg1*[ILC] mice compared to *Arg1*^{fl/fl} and *Arg1*^{+/+}*Il7t*[Cre/+] controls. Further, *Arg1*[ILC] mice exhibited reduced frequency of IL-5^{+} IL-13^{+} ILC2s compared to *Arg1*[flfl] mice (Fig. 4j,k), demonstrating that Arg1 expression is critical for optimal ILC2 cytokine effector function.

Although papain administration resulted in elevated numbers of CD45^{+} immune cells in the bronchoalveolar lavage fluid (BALF) of control mice (Fig. 4l), consisting primarily of eosinophils, this was significantly reduced in the absence of ILC-intrinsic Arg1 (Fig. 4l,m). Additionally, histological examination of the lungs revealed that although exposure to papain resulted in clusters of immune cell infiltrates (yellow arrows) and severe goblet cell hyperplasia (red arrows) in *Arg1*^{fl/fl} and *Arg1*^{+/+}*Il7t*[Cre/+] mice relative to PBS-treated controls, deletion of ILC-intrinsic Arg1 effectively blocked development of airway inflammation (Fig. 4n). Collectively, these results define an essential role for ILC-intrinsic Arg1 expression in promoting acute type 2 inflammation in the lung.

Arg1 regulates ILC2 responses in chronic lung inflammation

In addition to their role in regulating development of acute lung inflammation, ILC2s have also been implicated in the progression or resolution of chronic lung inflammation, including IPF[32] and helminth parasite-induced lung remodeling[33,34]. We next sought to test the involvement of ILC-derived Arg1 during chronic lung inflammation. Infection with the helminth parasite *Nippostrongylus brasiliensis* (Nb) leads to development of chronic lung inflammation, characterized by increased type 2 cytokines and heightened Arg1 expression[35,36]. Although *Arg1*^{fl/fl} mice exhibited a 2-fold increase in frequency of ILC2s in the inflamed lung one month post infection, loss of ILC-intrinsic Arg1 prevented generation of ILC2 responses (Supplementary Fig. 4a,b) and was associated with reduced *Arg1* expression in the inflamed lung (Supplementary Fig. 4c). Similarly, in a murine model of elastase enzyme instillation that leads to chronic damage to the alveolar septa partially mimicking the emphysematous pathology observed in COPD patients[37,38], we found that absence of ILC-intrinsic Arg1 prevented generation of robust ILC2 responses (Supplementary Fig. 4d,e), was associated with lower lung *Arg1* expression (Supplementary Fig. 4f) and reduced severity of emphysematous lung pathology (Supplementary Fig. 4g). Taken together, these data highlight a conserved role for ILC-intrinsic Arg1 in controlling ILC2 responses during both acute and chronic models of lung inflammation.

ILC3 function is independent of ILC-intrinsic Arg1

Expression of Arg1 is not restricted to the ILC2 lineage, as fetal RORγt[+] lymphoid tissue inducer (LTi) cells and a proportion of adult intestinal RORγt[+] LTi-like ILC3s have been reported to express Arg1-YFP[10]. Therefore, we next sought to test whether ILC-intrinsic Arg1 could regulate ILC3 responses in the steady-state or in the context of bacterial-induced intestinal inflammation. Examination of gut-associated RORγt[+] ILC3s and GATA3^{hi} ILC2s in *Arg1*^{fl/fl} and *Arg1*[ILC] mice revealed equivalent frequencies of total ILCs (Supplementary

Fig. 5a,b) and ILC3/ILC2 ratios (Supplementary Fig. 5c,d), suggesting that deletion of ILC-intrinsic Arg1 does not impair ILC3 development or homeostasis. To test whether ILC3 functionality is affected by the absence of ILC-intrinsic Arg1, mice were infected with the intestinal bacterium *Citrobacter rodentium* in which ILC3-derived IL-22 responses are critical mediators of host protection[39]. Although mice lacking RORγt^{+} cells (*RORc*(γt)[gfp/gfp]) or innate and adaptive lymphocytes (*Rag2*^{−/−}*Il2rg*^{−/−} and *Rag1*^{−/−}) succumbed to infection within two weeks post infection, *Arg1*^{fl/fl} and *Arg1* [ILC] mice did not exhibit any evidence of *Citrobacter*-induced inflammation or disease and survived infection (Supplementary Fig. 5e). Collectively, these data identify that Arg1 activity controls optimal ILC2, but not ILC3, responses.

Lung inflammation is independent of myeloid Arg1

In addition to ILCs, expression of Arg1 is an effector signature of AAMacs, although the functional significance of myeloid-derived Arg1 activity during type 2 inflammation in the lung remains controversial[19–23]. Fate-mapping analysis of *Il7r*[Cre/+]*Rosa26*[floxSTOP-eYFP] mice revealed that a minor population of macrophages were marked with a history of IL-7Rα expression (Fig. 5a) and only a small proportion of macrophages expressed Arg1-YFP during acute papain-induced inflammation (Fig. 5b). Flow cytometric analysis revealed no significant difference in macrophage frequencies (Fig. 5c) and equivalent expression of macrophage-intrinsic *Arg1* mRNA (Fig. 5d) and protein (Fig. 5e) expression were observed in the inflamed lungs of *Arg1*^{fl/fl} and *Arg1* [ILC] after papain exposure, indicating that AAMac accumulation and Arg1 expression are not impaired in *Arg1* [ILC] mice.

To test whether myeloid sources of Arg1 could act extrinsically to influence the magnitude of ILC2 responses and/or the development of papain-induced airway inflammation, we deleted Arg1 expression in macrophages and neutrophils using cre recombinase under control of the *Lyz2* (LysM) promoter (*Arg1* [Lyz2])[19,40]. Absence of Arg1 in LysM^{+} myeloid cells did not prevent generation of robust lung ILC2 responses to papain (Fig. 5f,g), nor did it influence the development of airway eosinophilia (Fig. 5h) or lung inflammation (Fig. 5i). Taken together, these results indicate a selective requirement for ILC-intrinsic Arg1 in the development of acute airway inflammation, revealing an unexpected degree of cellular specificity in the role of this enzyme in the lung.

Arg1 controls optimal ILC2 proliferation

The failure to mount a robust ILC2 response in the absence of cell-intrinsic Arg1 metabolic function could be due to impaired cell survival and/or reduced proliferative capacity. We found that deletion of Arg1 had no significant effect on the frequencies of 7AAD[+] Annexin V[+] apoptotic ILC2s in the lungs of PBS- or papain-treated mice (Supplementary Fig. 6a–c), suggesting that the absence of ILC-intrinsic Arg1 does not influence ILC2 survival under homeostatic conditions or during acute lung inflammation. To test whether loss of Arg1 could affect ILC2 proliferation, we examined intracellular expression of the proliferation marker Ki67 in ILC2s isolated *ex vivo* during acute papain-induced lung inflammation. A high proportion of lung ILC2s from *Arg1*^{fl/fl} and *Arg1*^{+/+}*Il7r*[Cre/+] mice were Ki67^{+} (38–44%) (Fig. 6a,b), indicative of these mice mounting a strong effector response to the papain allergen. In contrast, deletion of ILC-intrinsic Arg1 severely restrained ILC2 proliferation,

resulting in significantly reduced frequencies (Fig. 6a,b) and cell numbers (Fig. 6c) of Ki67^{+} ILC2s. To test directly whether cell-intrinsic Arg1 enzymatic activity was required to regulate ILC2 proliferation, we sort-purified activated ILC2s from wild type mice treated with recombinant murine IL-33 (rmIL-33) and tracked cellular divisions in the presence or absence of the selective Arginase 1 inhibitor N[ω]-hydroxy-nor-Arginine (nor-NOHA) (Fig. 6d). Within 48 hours, nearly 80% of the ILC2s treated with control DMSO had undergone at least one division and over 20% had reached 3–5 divisions (Fig. 6e,f). In contrast, Arg1 enzymatic inhibition resulted in greatly reduced cellular division with more than 45% of the cells remaining undivided (Fig. 6e,f). Consistent with our *in vivo* papain studies, the failure of the nor-NOHA-treated cells to divide was not associated with enhanced cell death (Supplementary Fig. 6d). Collectively, these studies demonstrate an essential role for Arg1 enzymatic activity in controlling the maximal proliferative capacity, but not survival, of activated ILC2s.

Arg1 inhibition disrupts amino acid metabolism

Arginine can be catabolized through several enzymatic pathways to yield a diverse set of metabolic intermediates that serve as substrates for downstream cellular and bioenergetic processes (Supplementary Fig. 7a and ref[11,31,41,42]). We hypothesized that the failure of Arg1-deficient ILC2s to proliferate may be associated with an imbalance in these metabolic substrates due to the disruption of Arg1 activity and potential compensation by the other enzymatic pathways to catabolize the excess arginine in its absence. To examine this, we first cultured IL-33-activated ILC2s in the presence or absence of the Arg1 inhibitor nor-NOHA and measured the relative abundance of metabolites using liquid chromatography mass spectrometry (Supplementary Fig. 7b). As expected, inhibition of Arg1 resulted in increased arginine in nor-NOHA-treated cells (Fig. 7a), confirming that ILC2s express functional Arg1 enzyme. Although DMSO-treated cells exhibited high abundance of the immediate downstream products ornithine and proline, amounts of these metabolites were severely diminished by Arg1 inhibition (Fig. 7b,c). We did not observe any corresponding increase in metabolites associated with two other main arginine catabolic pathways that would generate either citrulline-argininosuccinate via nitric oxide synthase (NOS) (Fig. 7d) or creatine-creatinine biosynthesis via L-Arginine:glycine amidinotransferase (AGAT) (Fig. 7e), suggesting that excess arginine is likely not diverted through these pathways to compensate for the absence of Arg1.

Changes in a metabolite pool size can result from either altered production or altered consumption rate within the cell[41,43]. Therefore, in order to further examine the metabolic fate of arginine in activated ILC2s, we traced the incorporation of a uniformly-enriched U-^{13}C-L-arginine isotope in ILC2s in the presence or absence of Arg1. While DMSO-treated ILC2s exhibited rapid and almost complete entry of labeled [13]C L-arginine into ornithine (Fig. 7f,g) and proline (Fig. 7h,i) quickly reaching saturation kinetics, inhibition of Arg1 severely diminished this process, indicating that this amino acid is the primary precursor for both molecules in activated ILC2s. Further, inhibition of Arg1 activity also resulted in severely diminished entry of [13]C L-arginine into the biosynthesis of ornithine-derived polyamine metabolite spermidine (Fig. 7j,k). Notably, reversible interconversion between proline and ornithine metabolite pools is a well-appreciated reaction in mammalian

cells[42], thereby supporting the conclusion that ornithine-derived polyamines, rather than ornithine and proline themselves, are a primary fate of L-arginine catabolism in ILC2s.

Taken together, these data indicate a model in which disruption of Arg1 in ILC2s is not associated with enhanced NOS or AGAT metabolism (Supplementary Fig. 7a, black arrows) but instead prevents generation of L-arginine-derived polyamines (Supplementary Fig. 7a, green arrows), molecules that are known to regulate cell growth and survival[31,41].

Arg1 regulates maximal ILC2 glycolytic capacity

Proteins are just one component of a diverse set of nutrient substrates that immune cells can use to fuel their growth[7,44], raising the question of whether Arg1 metabolism influences bioenergetic pathways in addition to amino acid catabolism. Particularly, the induction of aerobic glycolysis is a hallmark of effector lymphocyte metabolism[7] although whether this reprogramming is employed by ILCs during activation has never been examined. First, to characterize the different bioenergetic pathways utilized by ILC2s during activation, we sort purified lung IL-33R$^+$ ILC2s and T_H2 cells from mice treated with rmIL-33 (Fig. 8a) and measured cellular oxygen consumption rate (OCR) and extracellular acidification rate (ECAR), indicators of mitochondrial respiration and aerobic glycolysis, respectively. ILC2s exhibited both elevated spare respiratory capacity (SRC) (Fig. 8b,c) and high ECAR (Fig. 8d,e) in comparison to T_H2 cells, suggesting that ILC2s possess the capacity to augment mitochondrial respiration above basal conditions compared to T_H2 cells and highly engage aerobic glycolysis. To test specifically whether Arg1 enzymatic activity could influence the respiratory or glycolytic capacity of ILC2s, we activated lung ILC2s with rmIL-33 *in vivo* and treated the cells *ex vivo* with nor-NOHA to inhibit Arg1 activity during measurement of ECAR and OCR. ILC2 spare respiratory capacity was not substantially affected by Arg1 inhibition (Fig. 8f,g), suggesting that this enzyme does not significantly affect oxidative phosphorylation in ILC2s. In contrast, inhibition of Arg1 effectively abolished the ability of ILC2s to utilize aerobic glycolysis, resulting in severely diminished maximal glycolytic capacity (Fig. 8h,i), indicating a critical regulatory role for Arg1 in influencing glucose metabolism in activated ILC2s.

Together with the trace analysis of arginine metabolites, these data provide evidence for a previously unrecognized function for this biochemical pathway in which Arg1 enzymatic activity acts on multiple biosynthetic and bioenergetic pathways to function as a metabolic checkpoint that controls ILC2 proliferation and effector function that drives type 2 inflammation.

Discussion

ILC2s can promote pathologic inflammation or host-protective tissue repair in the lung following activation by cell-extrinsic environmental cues including alarmins and cytokines[1,2]. Here we demonstrate an essential role for cell-intrinsic Arg1 expression in regulating the proliferation and effector function of ILC2s required to promote acute and chronic type 2 airway inflammation. Inhibition of Arg1 enzymatic activity disrupted multiple components of ILC2 metabolic programming via altering arginine catabolism and

limiting aerobic glycolysis, indicating that Arg1 enzymatic activity serves as an essential checkpoint controlling ILC2 metabolism and the development of type 2 inflammation.

Unlike macrophage-derived Arg1 expression that requires induction by type 2 cytokines[15,16], we found that Arg1 is constitutively expressed in bone marrow ILC2 progenitors and maintained in mature cells across diverse tissue environments, provoking the question of when Arg1 is turned on during ILC development. Although HSCs, CLPS and the common ILC progenitor CHILP did not express Arg1, examination of an ILC2 lineage-committed bone marrow precursor lacking KLRG1 (ILC2P)[24] exhibited Arg1 expression equivalent to mature ILC2s. This upregulation of Arg1 expression in ILC2Ps occurred before the cells express transcripts for effector cytokines IL-5 and IL-13[24], which may provide a rationale for why a previous study using IL-5 promoter-driven Cre to delete Arg1 observed no significant effects on ILC2 responses[9]. Of note, the constitutive Arg1 expression in ILC2s is independent of IL-4- or IL-13-STAT6 signaling[9], leaving the molecular and cytokine cues that induce Arg1 expression requiring further investigation.

Until the identification of ILC2s as a constitutive source of Arg1, expression of this enzyme was thought to be a defining trait of the myeloid lineage, particularly AAMacs where it serves to regulate wound healing, fibrosis and suppression of T cell responses[11,14–16]. Our study suggests an unexpected degree of cellular specificity in the role of this enzyme, as deletion of myeloid cell sources of Arg1 via *Lyz2* promoter-driven expression of Cre recombinase did not affect ILC2 responses or dampen papain-induced airway inflammation. Although the reasons for this cellular compartmentalization of Arg1 function require further analysis, it may provide a rationale for reconciling paradoxical reports of the role of Arg1 during type 2 lung inflammation. Previous studies using deletion of myeloid cell-restricted Arg1 have failed to recapitulate the effects observed when global chemical inhibition or absence of hematopoietic cell-restricted Arg1 can dampen airway inflammation[19–23]. The data presented here demonstrate that deletion of ILC-intrinsic Arg1 acts to limit the magnitude of the ILC2 response itself, thereby diminishing their pro-inflammatory capacity and preventing the development of acute and chronic type 2 inflammation in the lung. Notably, myeloid cell-intrinsic Arg1 expression must be induced via AAMac polarization, a process that is partially dependent on ILC2-derived type 2 cytokines[45,46], thus revealing an additional indirect mechanism by which ILC2s control Arg1 metabolism during inflammatory conditions.

Elevated ILC2 responses have been reported in a number of human inflammatory disorders of the intestine, skin and lung barrier sites[1]. Particularly within the lung, dysregulation of L-arginine metabolism and Arg1 expression have been observed in patients diagnosed with inflammatory diseases including asthma[25–28] as well as COPD[29,30] and IPF[17]. Further, L-arginine dietary supplementation or chemical inhibition of Arg activity are being evaluated as clinical therapies for the treatment of asthma[25,26,28]. Despite these clinical correlations, the mechanisms by which this enzyme regulates lung inflammation are incompletely understood and assumed to be largely due to a reciprocal effect of increased nitric oxide and smooth muscle contractility in the absence of Arg1[26,30]. Further, the identities of the sources of human Arg1 are controversial and incompletely defined. Using primary lung tissue from patients with COPD and IPF, our study revealed selective expression of Arg1 on IL-33R⁺

ILC2 populations but not other ILC subsets. Although the significance of this restricted expression pattern is not yet clear, IL-33R expression is strongly enhanced on human ILC2s in response to cytokine signals[47] and therefore may represent a more activated state ILC2s gain in inflamed tissue. Taken together with the murine mechanistic data, our studies suggest that Arg1 metabolic control of ILC2 function is a critical determinant of both acute and chronic type 2 inflammation in the lung and thus represents a previously unrecognized axis for targeted therapeutics.

Despite constitutive expression of Arg1 in ILC2 bone marrow progenitors, the absence of Arg1 did not appear to affect ILC2 development or maturation. Instead, Arg1 activity influenced the ability of these cells to proliferate and exert their pro-inflammatory function upon activation. This suggests a clear demarcation in the role of this enzyme in regulating the inflammatory but not homeostatic state of ILC2s, perhaps due to the differential metabolic requirements of proliferating cells versus those at rest. Inhibition of Arg1 and the subsequent decreased catabolism of arginine into ornithine resulted in an imbalance of amino acid metabolites, especially the reduced synthesis of polyamines from L-arginine. Polyamine metabolites have been linked to diverse biological processes including proliferation, apoptosis and cellular stress responses[31,41] and further biochemical studies will be required to investigate the fates of these molecules in ILC2 biology.

Amino acids are one member of a large array of nutrients utilized for cell growth[7,44], provoking the question of whether Arg1 influences other aspects of ILC2 metabolic programming. We found the effect of Arg1 was not limited to arginine catabolism but also resulted in a severe block in the ability of these cells to employ maximal rates of aerobic glycolysis (also known as Warburg metabolism[7,8]) to fuel proliferation. Although the effects of Arg1 on arginine and glucose metabolism may not be directly linked and likely involve a complex imbalance of many metabolic intermediates, it is remarkable that disruption of a single urea cycle enzyme profoundly influences such distinct metabolic pathways and may offer a new understanding of the importance of this enzyme beyond the classical urea cycle. As both a constitutive and inflammatory source of arginase, ILC2s appear to occupy a unique functional niche mimicking both Arg1-dependent homeostatic hepatocyte function and inflammation-induced myeloid cell function. Critically however, mammalian survival depends on hepatocyte-intrinsic Arg1 expression above any hematopoietic source[12,31], perhaps reflecting an evolutionary compartmentalization of arginase activity that fulfills the primary biological need of mammals for urea production while also limiting the pro-inflammatory consequences of Arg1-driven ILC2 activation. Understanding how Arg1 metabolism integrates into the broader metabolic networks that govern the ability of ILCs and other innate immune cells to meet the biosynthetic and bioenergetic demands created during tissue inflammation may reveal new therapeutic targets for the treatment of multiple human inflammatory and metabolic diseases.

Methods

Mice

C57BL/6J (wild type, WT) mice were purchased from the Jackson Laboratory. $Arg1^{fl/fl}$, $Lyz2$-cre, $RORc(\gamma t)^{gfp/gfp}$, $Foxp3^{eGFP}$, $Rag1^{-/-}$ and $Rosa26^{floxSTOP-eYFP}$ mice on a

C57BL/6J background were purchased from the Jackson Laboratory and bred in house. *Rag2*^{−/−} *Il2rg*^{−/−} mice were purchased from Taconic Farms (Hudson, NY). *Arg1*[YFP] mice on a C57BL/6 background[9,10] were generously provided by Richard Locksley (University of California San Francisco). *Il7r*[Cre/+] mice on a C57BL/6 background[48] were generously provided by Hans-Reimer Rodewald (German Cancer Research Center) and were used only as heterozygotes. For all cre-flox studies, littermate controls were used and animals were co-housed after weaning. Male and female mice were used at between 7–20 weeks of age. Within individual experiments, all animals were age- and sex-matched and exact number of animals used per experiment is indicated in figure legends. All mice were maintained in specific pathogen-free facilities at University of Pennsylvania or Weill Cornell Medicine. All protocols were approved by both the University of Pennsylvania and the Weill Cornell Medicine Institutional Animal Care and Use Committees (IACUC).

Models of lung and intestinal inflammation

For induction of acute type 2 airway inflammation, mice were anesthetized with Isothesia isoflurane, USP (Henry Schein Animal Health) and treated with 30 μg of papain (Calbiochem) or PBS intranasally (i.n.) in a volume of 30 μl every day for 5 days prior to sacrifice on day 6 for analysis. For induction of helminth-induced chronic type 2 inflammation, mice were anesthetized with Isothesia isoflurane, 500 L3 larvae of *Nippostrongylus brasiliensis* were injected subcutaneously, and animals were analyzed 30–32 days post infection. For induction of chronic emphysematous pathology, mice were anesthetized with Isothesia isoflurane, instilled with 3 units of elastase (Elastin Products Company) or PBS intratracheally and assessed at 30–35 days post treatment. For induction of intestinal inflammation, *Citrobacter rodentium* (formerly *Citrobacter freundii*, biotype 4280) strain DBS100 (provided by Bruce Vallance, University of British Columbia, Vancouver, British Columbia, Canada) was prepared by selecting a single colony and culturing in LB broth overnight as previously described[39]. Mice were inoculated with approximately 1×10^{10} colony forming units (CFU) in 200 μL via oral gavage.

Isolation of cells from mouse tissue

For isolation of cells from lymphoid tissues, tissues were pressed through 70 μm cell strainers using the plunger of a 3 ml syringe, washed with DMEM Wash Media (Dulbecco's modified Eagle's medium with 10% fetal bovine serum (Denville Scientific, Metuchen, NJ), 1% l-glutamine (GIBCO), 1% penicillin/streptomycin (GIBCO), and any remaining red blood cells were lysed. Isolation of cells from bone marrow was performed by flushing out the marrow from cleaned bones using a syringe containing DMEM Wash Media. Red blood cells were lysed with ACK buffer (Lonza). Isolation of cells from BALF and lung tissue was done as previously described[6]. Briefly, BALF cells were obtained by flushing the lungs with two washes of 1 ml cold PBS via a thin tube inserted into a cut made in the trachea. Lungs were then perfused with 10 ml PBS through the right ventricle of the heart prior to removal. Lung lobes were cut into small pieces using scissors and digested with 2 mg/ml Collagenase D (Roche) in PBS for 45 minutes at 37°C with vortexing every 10 minutes. Samples were pressed through 70 μm cell strainers, washed with DMEM Wash Media and any remaining red blood cells were lysed with ACK buffer. Isolation of lymphocytes from epididymal white adipose tissue (EWAT) was done as previously described[49]. Briefly, tissue was minced

with scissors and then digested with 1 mg/ml collagenase type II (Sigma-Aldrich) at 37°C with shaking at 200 rpm for 60–90 min. Digested tissues were passed through 70 μm cell strainers and washed with DMEM media. The adipocyte layer was removed after centrifugation and red blood cells were lysed with ACK buffer. Isolation of cells from the lamina propria of the large and small intestine was performed as previously described[50]. Single cell suspensions from all tissues were used for subsequent flow cytometry staining.

Isolation of cells from human lung tissue

Explanted lung tissue was collected from patients undergoing lung transplantation who elected to participate in the Prospective Registry of Outcomes in Patients Electing Lung Transplantation (PROPEL) study at the Hospital of the University of Pennsylvania. University of Pennsylvania Institutional review board approval and informed written consent from patients was obtained prior to recruitment. Single-cell suspensions of lung were prepared by chopping tissue into pieces with scissors, incubating the finely chopped tissue for 1 h with 2 mg/ml collagenase D (Roche) and 20 μg/ml DNase I (Roche) at 37°C with shaking at 200rpm, and mashing digested tissue through a wire mesh sieve. Liquid was passed through 70 μm cell strainers, underlaid with Ficoll-Paque (GE Healthcare), and centrifuged at 1600rpm for 20 minutes at room temperature with the brake off. White lymphocyte interface layer was removed and remaining red blood cells were lysed with ACK buffer. Cells were frozen in 90% FBS, 10% DMSO in a Nalgene Mr. Frosty container (Thermo Scientific). For flow cytomteric analysis, samples were thawed and stained as a single cohort to ensure consistency.

Flow cytometry

Single cell suspensions were stained with a combination of the following monoclonal fluorescently conjugated antibodies. All antibodies are from Affymetrix eBioscience unless specified otherwise. All antibodies were used at 1:200 dilution unless indicated otherwise. For murine studies: anti-mouse CD3 (145-2C11), CD4 (GK1.5), CD5 (53-7.3), CD11b (M1/70), CD11c (N418), CD19 (eBio1D3), CD25 (PC61.5), CD45 (30-F11), CD127 (A7R34), CD90.1 (HIS51), CD90.2 (53-2.1), IL-33R (DJ8, MD Bioproducts), NK1.1 (PK136), Siglec-F (E50-2440), CD103 (2E7), MHCII (M5/114.15.2) or Streptavidin (ebioscience, no clone). For mouse studies, Lineage negative gating (Lin−) includes markers for CD3, CD5, FcγR1, NK1.1, CD11b, B220, CD11c. For human studies: anti-human CD3 (OKT3), CD4 (OKT4), CD5 (UCHT2), CD14 (61D3), CD16 (CB16), CD19 (HIB19), CD56 (B159), CD25 (BC96), CD45 (HI30), CD127 (eBioRDR5; dilution 1:100), CRTH2 (BM16, BD Biosciences;dilution 1:50), FcεR1α (AER-37), or IL-33R (ST2L, B4E6, MD Bioproducts; dilution 1:100). The authors wish to note observation of substantial variability in staining efficiency between different lots of FITC anti-human IL-33R (ST2L) (MD Bioproducts). Staining efficacy should be validated for each individual lot.

For measurement of intracellular cytokine expression, cells were isolated *ex vivo* and stimulated in complete media (Dulbecco's modified Eagle's medium with 10% fetal bovine serum (Denville Scientific), 1% l-glutamine (GIBCO), 1% penicillin/streptomycin (GIBCO), 25 mm HEPES buffer, and 55 μm 2β-mercaptoethanol (Sigma-Aldrich)) with 50 ng/ml phorbol 12-myristate 13-acetate (Sigma-Aldrich), 500 ng/ml ionomycin (Sigma-Aldrich),

and 10 μg/ml brefeldin A (Sigma-Aldrich) for 4 h. Cells were subsequently surface stained with a combination of the antibodies listed above, fixed and permeabilized using a commercially available kit (BD Cytofix/Cytoperm, BD Biosciences), and stained with IL-13 Alexa Fluor 488 (eBioscience) and IL-5 PE (eBioscience).

For measurement of intracellular arginase, cells were isolated directly *ex vivo*, stained with antibodies against surface antigens, fixed and permeabilized according to manufacturer's instructions (BD Biosciences Cytofix/CytoPerm) and stained with sheep anti-Human/Mouse Arg1 FITC or PE (R&D Systems).

For analysis of transcription factor expression, cells were isolated directly *ex vivo*, stained with antibodies against surface antigens, fixed and permeabilized according to manufacturer's instructions (Foxp3/Transcription Factor Staining Buffer Set, eBioscience) and stained with PE-cojugated RORγt (B2D, eBioscience) and PerCP eFluor 710-conjugated GATA3 (TWAJ, eBioscience). Ki67 PE (BD Pharmigen), Annexin V FITC (BD Pharmigen), 7AAD (BD Via-Probe, BD Biosciences) staining were performed using commercially available kits (BD Biosciences).

For all stains except Annexin V and 7AAD analysis, dead cells were excluded from analysis by means of a viability stain (Live/Dead Fixable Aqua stain, Invitrogen). Samples were acquired on a custom configuration BD LSRII or BD Fortessa flow cytometer (BD Biosciences) and analyzed using FlowJo software (v9.2, Tree Star).

Cell Trace Assays

For analysis of cell division, C57BL/6J mice were treated with 100 ng of rmIL-33 (R&D Systems) intranasally every 3 days for 2–3 weeks. Lin$^-$CD45$^+$CD90$^+$CD25$^+$IL-33R$^+$ ILC2s were sort-purified from the lung and labeled with 5μM Cell Trace Violet (Invitrogen Molecular Probes). Cells were cultured for 48 h in DMEM Complete Media (Dulbecco's modified Eagle's medium with 10% fetal bovine serum (Denville Scientific), 1% l-glutamine (GIBCO), 1% penicillin/streptomycin (GIBCO), 25 mm HEPES buffer, and 55 μm 2-β-mercaptoethanol (Sigma-Aldrich)) with 20 ng/ml rmIL-2, 20 ng/ml rmIL-7, 50 ng/ml rmIL-33 (all cytokines from R&D Systems) with DMSO or 500μM nor-NOHA (Cayman Chemical) at 37°C. Dilution of cell trace violet dye was measured by flow cytometry.

RNA isolation and Real-Time Quantitative PCR

For analysis from lung tissue, lungs were perfused as described above and 2 small representative pieces from the right lobes placed in RNA*later* (QIAGEN). Tissue was later homogenized in RLT buffer and RNA was isolated using RNeasy mini kit according to manufacturer's instructions (QIAGEN). For analysis from purified immune cells, Lin$^-$CD45$^+$CD90$^+$CD25$^+$IL-33R$^+$ ILC2s or CD45$^+$CD11c$^+$F4/80$^+$ macrophages were sort-purified from WT mice treated with 30 μg papain for 5 days. Cells were sorted directly into TRIzol and RNA was isolated using chloroform extraction. For both methods, cDNA was generated using Superscript reverse transcription (Invitrogen). Real-time quantitative PCR (qRT-PCR) was performed on cDNA using SYBR green master mix (Applied Biosystems) and commercially available primer sets (QIAGEN). Reactions were run on a real-time PCR

system (ABI7500; Applied Biosystems). Samples were normalized to β-actin and displayed as a fold induction relative to expression levels in PBS-treated or naive tissue as indicated.

Tissue histological sections

Left lobes of lungs were inflated and fixed with 4% paraformaldehyde (bioWORLD), embedded in paraffin, and 5 μm sections were used for staining with hematoxylin and eosin (H&E) or periodic acid-Schiff (PAS). Image acquisition was performed using a Nikon Eclipse Ti microscope, a Nikon Digital Sight DS-Fi2 camera, and NIS-Elements AT version 4.2 acquisition software (Nikon). Adobe Photoshop (CS5, Adobe Systems Inc.) was used to adjust brightness and contrast only (changes were applied to the whole image).

Liquid chromatography mass spectrometry

Metabolite pool analysis—C57BL/6J mice were treated with 100 ng of rmIL-33 (R&D Systems) i.n. every 3 days for 2–3 weeks. $Lin^-CD45^+CD90^+CD25^+IL-33R^+$ ILC2s were sort-purified from the lung. 2×10^5 cells per well were cultured in a 96-well plate with DMEM Complete Media with 20 ng/ml rmIL-2, 20 ng/ml rmIL-7, 50 ng/ml rmIL-33 and DMSO or 500μM nor-NOHA at 37°C for 24 hours. Samples were harvested into eppendorf tubes, centrifuged at 5000 rpm for 5 min and cell were washed once with 1 ml ice-cold PBS. Cell pellets were resuspended in 1 mL 80% aqueous MeOH and stored at −80°C to promote protein precipitation. Extracts were clarified by centrifugation at 21,000 x g for 20 min at 4°C, dried using a Genevac benchtop evaporator (SP Industries) and reconstituted in 100 μL of 60:40 acetonitrile:water + 5 mM ammonium formate. Liquid chromoatography was performed using a 1290 HPLC system (Agilent Technologies) and Xbridge BEH Amide column (Waters Corporation; 150mm x 2.1mm, 3.5 μm). Samples were maintained at 4°C with 10 μL injection volume 200 μL/min LC flow rate. The aqueous mobile phase (A) was 0.1% formic acid in water, and the organic mobile phase (B) was 0.1% formic acid in acetonitrile. Initial conditions were 95% B with gradient program: 1.0 min: 95% B; 9.0 min: 50% B; 12.0 min: 25% B; 13.0 min: 25% B and 5 min re-equilibration time. Metabolite detection was using an Agilent 6550 Q-TOF with JetStream source operating in positive mode with gas temperature: 240°C; gas flow: 18 L/min; nebulizer pressure: 25 psig; sheath gas: 400°C and 11 L/min; VCap: 4000 V; Fragmentor: 300 V and continuous reference mass correction at m/z 121.05087 and 922.00980. Metabolites were identified by the combination of accurate mass and retention time relative to authentic standards and peak areas were extracted and integrated using Agilent MassHunter software.

Stable Isotope Tracing—C57BL/6J mice were treated with 100 ng of rmIL-33 i.n. every 3 days for 2–3 weeks. $Lin^-CD45^+ CD90^+CD25^+IL-33R^+$ ILC2s were sort-purified from the lung. 5×10^5 cells/ml were cultured in a 48-well plate with DMEM Complete Media with 20 ng/ml rmIL-2, 20 ng/ml rmIL-7, 50 ng/ml rmIL-33 and DMSO or 500μM nor-NOHA at 37°C for 36 hours. Samples were centrifuged at 1600 rpm for 5 min and washed once with ice-cold PBS. Cells were then cultured at a concentration of 3.3×10^5 cells/ml in arginine-free, lysine-free, high glucose DMEM media (GIBCO, formulation A14431) supplemented with 10% dialyzed fetal bovine serum (GIBCO), 1% l-glutamine, 1% penicillin/streptomycin, 25 mm HEPES buffer, 55 μm 2-β-mercaptoethanol, 0.80 mM lysine and 0.4 mM U-^{13}C-L-arginine (Cambridge Isotopes). Cells were harvested at the indicated time

points by centrifugation at 5000 rpm for 5 min and prepared for LC-MS analysis as above. Extracted ion chromatograms for all mass isotopomers were generated using Agilent MassHunter software and corrected for natural abundance using IsoCor software[43].

Seahorse cellular metabolic profiling—$Foxp3^{eGFP}$ reporter mice were treated with 100 ng of rmIL-33 (R&D Systems) i.n. every 3 days for 2–3 weeks. Lin^- $CD45^+CD90^+CD25^+IL$-$33R^+$ ILC2s and/or $CD45^+CD3^+CD5^+CD4^+Foxp3^-IL$-$33R^+$ T_H2 cells were sort-purified from the lung and rested for 18 h in DMEM Complete Media (Dulbecco's modified Eagle's medium with 10% fetal bovine serum (Denville Scientific), 1% l-glutamine (GIBCO), 1% penicillin/streptomycin (GIBCO), 25 mm HEPES buffer, and 55 μm 2-β-mercaptoethanol (Sigma-Aldrich)) on ice. For Arg1 inhibitor studies only, cells were then cultured for additional 24 hin DMEM Complete Media with 20 ng/ml rIL-2, 20 ng/ml rIL-7 and 50 ng/ml rIL-33 (all cytokines from R&D Systems) at 37°C. Cells were plated at 200,000 cells per well and OCR and ECAR measured in XF media (non-buffered RPMI 1640 containing 25 mM glucose, 2 mM L-glutamine, and 1 mM sodium pyruvate) under basal conditions, in response to 1 μM oligomycin, 1.5 μM fluoro-carbonyl cyanicide phenylhydrazone (FCCP) and 100 nM rotenone + 1 μM antimycin A (Sigma-Aldrich) and as indicated after DMSO or 500 μM nor-NOHA injection using a 96 well Extracellular Flux Analyzer (Seahorse Bioscience).

Statistical analysis—Results represent the mean ± SEM unless indicated otherwise. Statistical significance was determined by test as indicated in figure legends. Statistical analyses were performed using Prism GraphPad software v5.0. Researchers were not blinded to experimental groups. Exclusion criteria were not applied as no experimental samples were excluded from analysis.

Supplementary Material

Refer to Web version on PubMed Central for supplementary material.

Acknowledgments

References

1. Artis D, Spits H. The biology of innate lymphoid cells. Nature. 2015; 517:293–301. [PubMed: 25592534]

2. McKenzie AN, Spits H, Eberl G. Innate lymphoid cells in inflammation and immunity. Immunity. 2014; 41:366–374. [PubMed: 25238094]

3. Chang YJ, et al. Innate lymphoid cells mediate influenza-induced airway hyper-reactivity independently of adaptive immunity. Nat Immunol. 2011; 12:631–638. [PubMed: 21623379]

4. Barlow JL, et al. Innate IL-13-producing nuocytes arise during allergic lung inflammation and contribute to airways hyperreactivity. J Allergy Clin Immunol. 2012; 129:191–198. e194. [PubMed: 22079492]

5. Halim TY, et al. Group 2 innate lymphoid cells are critical for the initiation of adaptive T helper 2 cell-mediated allergic lung inflammation. Immunity. 2014; 40:425–435. [PubMed: 24613091]

6. Monticelli LA, et al. Innate lymphoid cells promote lung-tissue homeostasis after infection with influenza virus. Nat Immunol. 2011; 12:1045–1054. [PubMed: 21946417]

7. Buck MD, O'Sullivan D, Pearce EL. T cell metabolism drives immunity. J Exp Med. 2015; 212:1345–1360. [PubMed: 26261266]

8. Vander Heiden MG, Cantley LC, Thompson CB. Understanding the Warburg effect: the metabolic requirements of cell proliferation. Science. 2009; 324:1029–1033. [PubMed: 19460998]

9. Bando JK, Nussbaum JC, Liang HE, Locksley RM. Type 2 innate lymphoid cells constitutively express arginase-I in the naive and inflamed lung. J Leukoc Biol. 2013; 94:877–884. [PubMed: 23924659]

10. Bando JK, Liang HE, Locksley RM. Identification and distribution of developing innate lymphoid cells in the fetal mouse intestine. Nat Immunol. 2015; 16:153–160. [PubMed: 25501629]

11. Rath M, Muller I, Kropf P, Closs EI, Munder M. Metabolism via Arginase or Nitric Oxide Synthase: Two Competing Arginine Pathways in Macrophages. Front Immunol. 2014; 5:532. [PubMed: 25386178]

12. Thomas AC, Mattila JT. "Of mice and men": arginine metabolism in macrophages. Front Immunol. 2014; 5:479. [PubMed: 25339954]

13. Murray PJ. Amino acid auxotrophy as a system of immunological control nodes. Nat Immunol. 2015; 17:132–139. [PubMed: 26784254]

14. Raber P, Ochoa AC, Rodriguez PC. Metabolism of L-arginine by myeloid-derived suppressor cells in cancer: mechanisms of T cell suppression and therapeutic perspectives. Immunol Invest. 2012; 41:614–634. [PubMed: 23017138]

15. Wynn TA, Chawla A, Pollard JW. Macrophage biology in development, homeostasis and disease. Nature. 2013; 496:445–455. [PubMed: 23619691]

16. Murray PJ, Wynn TA. Protective and pathogenic functions of macrophage subsets. Nat Rev Immunol. 2011; 11:723–737. [PubMed: 21997792]

17. Gibbons MA, et al. Ly6Chi monocytes direct alternatively activated profibrotic macrophage regulation of lung fibrosis. Am J Respir Crit Care Med. 2011; 184:569–581. [PubMed: 21680953]

18. Rodriguez PC, Quiceno DG, Ochoa AC. L-arginine availability regulates T-lymphocyte cell-cycle progression. Blood. 2007; 109:1568–1573. [PubMed: 17023580]

19. Pesce JT, et al. Arginase-1-expressing macrophages suppress Th2 cytokine-driven inflammation and fibrosis. PLoS Pathog. 2009; 5:e1000371. [PubMed: 19360123]

20. Barron L, et al. Role of arginase 1 from myeloid cells in th2-dominated lung inflammation. PLoS One. 2013; 8:e61961. [PubMed: 23637937]

21. Cloots RH, et al. Ablation of Arg1 in hematopoietic cells improves respiratory function of lung parenchyma, but not that of larger airways or inflammation in asthmatic mice. Am J Physiol Lung Cell Mol Physiol. 2013; 305:L364–376. [PubMed: 23831616]

22. North ML, Khanna N, Marsden PA, Grasemann H, Scott JA. Functionally important role for arginase 1 in the airway hyperresponsiveness of asthma. Am J Physiol Lung Cell Mol Physiol. 2009; 296:L911–920. [PubMed: 19286931]

23. Yang M, et al. Inhibition of arginase I activity by RNA interference attenuates IL-13-induced airways hyperresponsiveness. J Immunol. 2006; 177:5595–5603. [PubMed: 17015747]

24. Hoyler T, et al. The transcription factor GATA-3 controls cell fate and maintenance of type 2 innate lymphoid cells. Immunity. 2012; 37:634–648. [PubMed: 23063333]

25. Lara A, et al. Alterations of the arginine metabolome in asthma. Am J Respir Crit Care Med. 2008; 178:673–681. [PubMed: 18635886]

26. Bratt JM, Zeki AA, Last JA, Kenyon NJ. Competitive metabolism of L-arginine: arginase as a therapeutic target in asthma. J Biomed Res. 2011; 25:299–308. [PubMed: 23554705]

27. Holguin F, et al. An association between L-arginine/asymmetric dimethyl arginine balance, obesity, and the age of asthma onset phenotype. Am J Respir Crit Care Med. 2013; 187:153–159. [PubMed: 23204252]

28. Vonk JM, et al. Arginase 1 and arginase 2 variations associate with asthma, asthma severity and beta2 agonist and steroid response. Pharmacogenet Genomics. 2010; 20:179–186. [PubMed: 20124949]

29. Bergeron C, et al. Influence of cigarette smoke on the arginine pathway in asthmatic airways: increased expression of arginase I. J Allergy Clin Immunol. 2007; 119:391–397. [PubMed: 17291856]

30. Tadie JM, et al. Role of nitric oxide synthase/arginase balance in bronchial reactivity in patients with chronic obstructive pulmonary disease. Am J Physiol Lung Cell Mol Physiol. 2008; 294:L489–497. [PubMed: 17675371]

31. Wu G, et al. Arginine metabolism and nutrition in growth, health and disease. Amino Acids. 2009; 37:153–168. [PubMed: 19030957]

32. Hams E, et al. IL-25 and type 2 innate lymphoid cells induce pulmonary fibrosis. Proc Natl Acad Sci U S A. 2014; 111:367–372. [PubMed: 24344271]

33. Turner JE, et al. IL-9-mediated survival of type 2 innate lymphoid cells promotes damage control in helminth-induced lung inflammation. J Exp Med. 2013; 210:2951–2965. [PubMed: 24249111]

34. Tait Wojno ED, et al. The prostaglandin D2 receptor CRTH2 regulates accumulation of group 2 innate lymphoid cells in the inflamed lung. Mucosal Immunol. 2015; 8:1313–1323. [PubMed: 25850654]

35. Reece JJ, Siracusa MC, Scott AL. Innate immune responses to lung-stage helminth infection induce alternatively activated alveolar macrophages. Infect Immun. 2006; 74:4970–4981. [PubMed: 16926388]

36. Marsland BJ, Kurrer M, Reissmann R, Harris NL, Kopf M. Nippostrongylus brasiliensis infection leads to the development of emphysema associated with the induction of alternatively activated macrophages. Eur J Immunol. 2008; 38:479–488. [PubMed: 18203142]

37. Fujita M, Nakanishi Y. The pathogenesis of COPD: lessons learned from in vivo animal models. Med Sci Monit. 2007; 13:RA19–24. [PubMed: 17261992]

38. Demkow U, van Overveld FJ. Role of elastases in the pathogenesis of chronic obstructive pulmonary disease: implications for treatment. Eur J Med Res. 2010; 15(Suppl 2):27–35. [PubMed: 21147616]

39. Sonnenberg GF, Monticelli LA, Elloso MM, Fouser LA, Artis D. CD4(+) lymphoid tissue-inducer cells promote innate immunity in the gut. Immunity. 2011; 34:122–134. [PubMed: 21194981]

40. Knippenberg S, Brumshagen C, Aschenbrenner F, Welte T, Maus UA. Arginase 1 activity worsens lung-protective immunity against Streptococcus pneumoniae infection. Eur J Immunol. 2015; 45:1716–1726. [PubMed: 25789453]

41. Miller-Fleming L, Olin-Sandoval V, Campbell K, Ralser M. Remaining Mysteries of Molecular Biology: The Role of Polyamines in the Cell. J Mol Biol. 2015; 427:3389–3406. [PubMed: 26156863]

42. Phang JM, Liu W, Hancock CN, Fischer JW. Proline metabolism and cancer: emerging links to glutamine and collagen. Curr Opin Clin Nutr Metab Care. 2015; 18:71–77. [PubMed: 25474014]

43. Millard P, Letisse F, Sokol S, Portais JC. IsoCor: correcting MS data in isotope labeling experiments. Bioinformatics. 2012; 28:1294–1296. [PubMed: 22419781]

44. van der Windt GJ, Pearce EL. Metabolic switching and fuel choice during T-cell differentiation and memory development. Immunol Rev. 2012; 249:27–42. [PubMed: 22889213]

45. Molofsky AB, et al. Innate lymphoid type 2 cells sustain visceral adipose tissue eosinophils and alternatively activated macrophages. J Exp Med. 2013; 210:535–549. [PubMed: 23420878]

46. Li D, et al. IL-33 promotes ST2-dependent lung fibrosis by the induction of alternatively activated macrophages and innate lymphoid cells in mice. J Allergy Clin Immunol. 2014; 134:1422–1432. e1411. [PubMed: 24985397]

47. Xue L, et al. Prostaglandin D2 activates group 2 innate lymphoid cells through chemoattractant receptor-homologous molecule expressed on TH2 cells. J Allergy Clin Immunol. 2014; 133:1184–1194. [PubMed: 24388011]

48. Schlenner SM, et al. Fate mapping reveals separate origins of T cells and myeloid lineages in the thymus. Immunity. 2010; 32:426–436. [PubMed: 20303297]

49. Brestoff JR, et al. Group 2 innate lymphoid cells promote beiging of white adipose tissue and limit obesity. Nature. 2015; 519:242–246. [PubMed: 25553952]

50. Osborne LC, et al. Coinfection. Virus-helminth coinfection reveals a microbiota-independent mechanism of immunomodulation. Science. 2014; 345:578–582. [PubMed: 25082704]
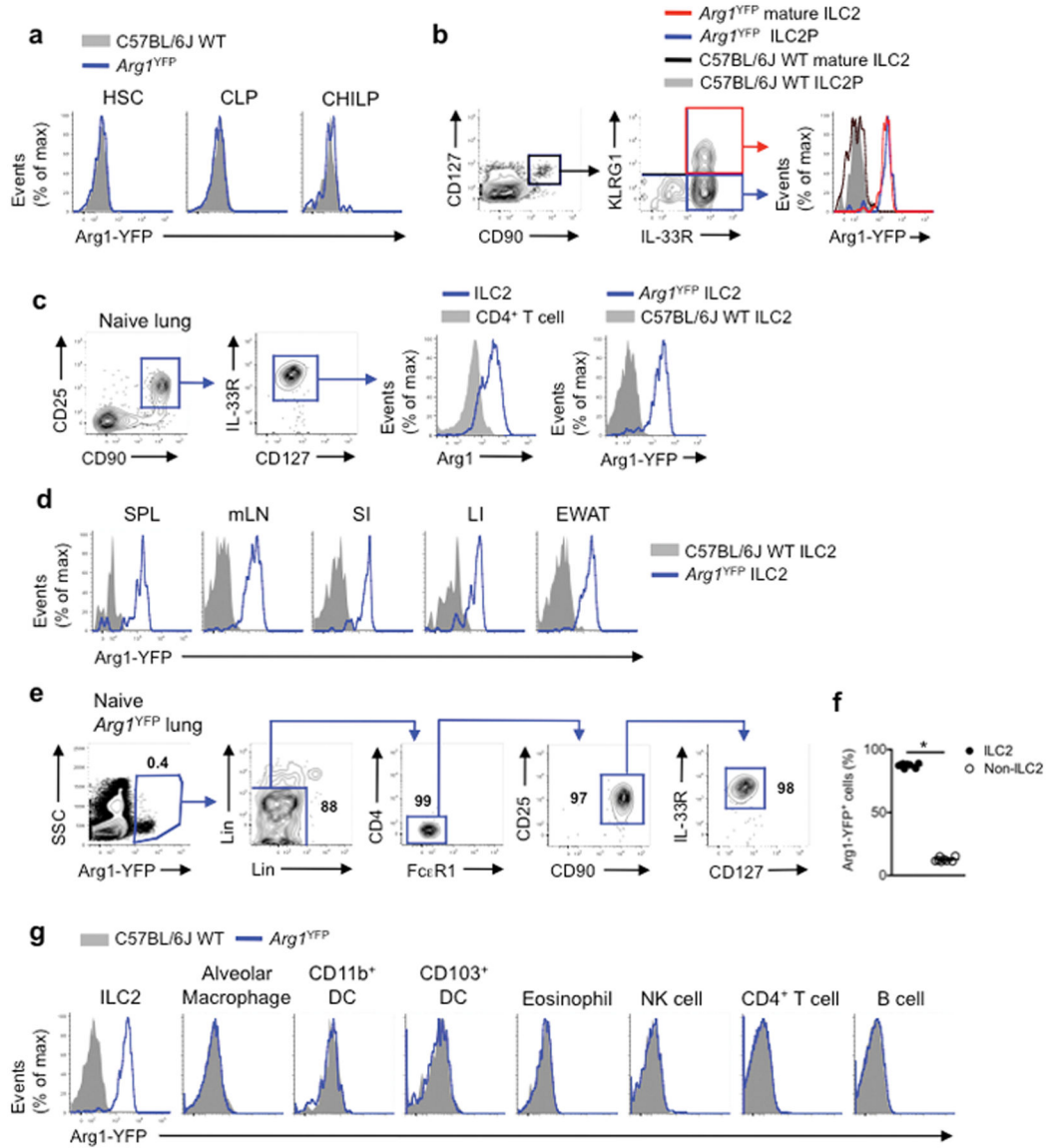
Figure 1. Constitutive Arg1 expression is a conserved trait of precursor and mature ILC2s across diverse tissue sites

(**a**) Flow cytometric analysis of Arginase 1 (Arg1-YFP) expression in bone marrow HSC (Lin$^-$CD90$^-$CD127$^-$c-kit^{hi}Sca-1^{hi}); CLP (Lin$^-$CD90$^-$CD127$^+$ CD25$^-$α4β7$^-$Flt3$^+$Sca-1^{lo}c-kit^{lo}); common ILC progenitor CHILP (Lin$^-$CD90$^-$CD127$^+$α4β7$^+$Flt3$^-$) from *Arg1*^{YFP} mice. (**b**) Flow cytometric analysis of Arg1-YFP expression in immature ILC2Ps (Lin$^-$CD127$^+$CD90$^+$IL-33R$^+$KLRG1$^-$) and mature ILC2s (Lin$^-$CD127$^+$CD90$^+$IL-33R$^+$KLRG1$^+$). (**c**) Flow cytometric analysis of Arg1 expression in mature ILC2s (Lin$^-$CD45$^+$CD90$^+$CD25$^+$IL-33R$^+$) from naive lung tissue of C57BL/6J wildtype (WT) mice or *Arg1*^{YFP} mice. (**d**) Flow cytometric analysis of Arg1-YFP expression in mature ILC2s (Lin$^-$CD45$^+$CD90$^+$CD127$^+$IL-33R$^+$KLRG1$^+$) from spleen (SPL), mesenteric lymph node (mLN), small intestine lamina propria (SI), large intestine lamina propria (LI) and epididymal white adipose tissue (EWAT) from naive *Arg1*^{YFP} and

WT mice. (**e**) Sequential flow cytometric gating in $Arg1^{YFP}$ naive lung tissue. Lineage negative gating (Lin) includes markers for CD3, CD5, FcεR1, NK1.1, CD11b, B220, CD11c. (**f**) Quantification of the relative frequency of Arg1-YFP$^+$ ILC2s versus all other cell populations (called Non-ILC2) in naive lung tissue of $Arg1^{YFP}$ mice. (**g**) Representative flow cytometric plots of Arg1-YFP expression in ILC2s (Lin$^-$CD45$^+$CD90$^+$CD25$^+$IL-33R$^+$), alveolar macrophages (CD11b$^+$CD11c$^+$F4/80$^+$Ly6G$^-$CD3$^-$CD19$^-$), CD11b$^+$ DCs (CD103$^-$CD11b$^+$CD11c$^+$F4/80$^-$MHCII$^+$), CD103$^+$ DCs (CD103$^+$CD11b$^-$CD11c$^+$F4/80$^-$MHCII$^+$), eosinophils (CD11b$^+$Siglec F$^+$CD11c$^-$), NK cells (CD3$^-$NK1.1$^+$), CD4 T cells (CD3$^+$CD4$^+$) and B cells (CD3$^-$CD19$^+$). All data are representative of three independent experiments with similar results. N = 3 mice per group except (**e**) in which n = 8 mice. Data shown are the mean ± SEM. * p < 0.001 as determined by unpaired Student's t test.
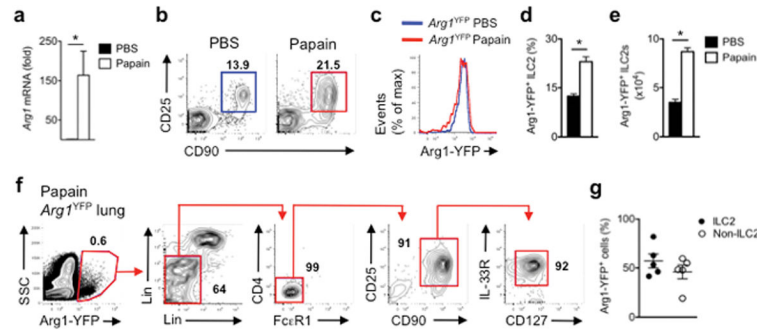
Figure 2. ILC2s are a main source of Arg1 in the lung during type 2 inflammation
(**a**) WT mice were treated with 30 μg papain or PBS intranasally (i.n.) for 5 days and analyzed on day 6 for *Arg1* mRNA expression in lung tissue, determined by RT-PCR and shown relative to levels in PBS-treated control mice. (**b–g**) WT or *Arg1*[YFP] mice were treated with 30 μg papain or PBS i.n. for 5 days and analyzed on day 6. (**b**) Representative flow cytometric plots of lung ILC2 frequencies in PBS or papain-treated WT mice, pregated on Lin⁻ CD45⁺ cells. (**c**) Arg1-YFP expression in lung ILC2s from PBS or papain-treated *Arg1*[YFP] mice. Numbers represent mean fluorescence intensity (MFI) of Arg1-YFP expression levels. (**d**) Frequency and (**e**) cell number of Arg1-YFP⁺ ILC2s in PBS or papain-treated mice at day 6. (**f**) Sequential flow cytometric gating of Arg1-YFP expression in lung tissue from papain-treated mice. Lineage negative gating (Lin) includes markers for CD3, CD5, NK1.1, CD11b, B220, CD11c. (**g**) Quantification of the relative frequency of Arg1-YFP⁺ ILC2s versus non-ILC2 populations in papain-treated lung tissue of *Arg1*[YFP] mice. All data are representative of three independent experiments with similar results. N = 3 mice per group (**a–e**) or n = 5 mice per group (**f,g**). Data shown are the mean ± SEM. * p < 0.001 as determined by unpaired Student's *t* test.
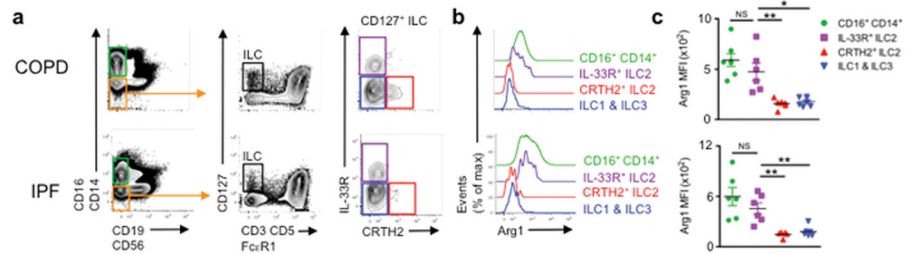
Figure 3. Human ILC2s express Arg1 during chronic lung disease

(**a**) Flow cytometric analysis of lung explant tissue from patients with COPD or IPF identifying Lin⁻CD127⁺ ILC subsets expressing IL-33R or CRTH2. (**b**) Mean fluorescence intensity (MFI) of intracellular Arg1 expression in cell subsets. (**c**) Quantification of Arg1 MFI per cell subset. Data shown in (**a**) and (**b**) are representative of 6 COPD and 7 IPF tissue samples analyzed as part of one experiment. Data shown in (**c**) are the mean ± SEM. $*p < 0.05$, $**p < 0.01$, as determined by two-way ANOVA. NS, not significant.
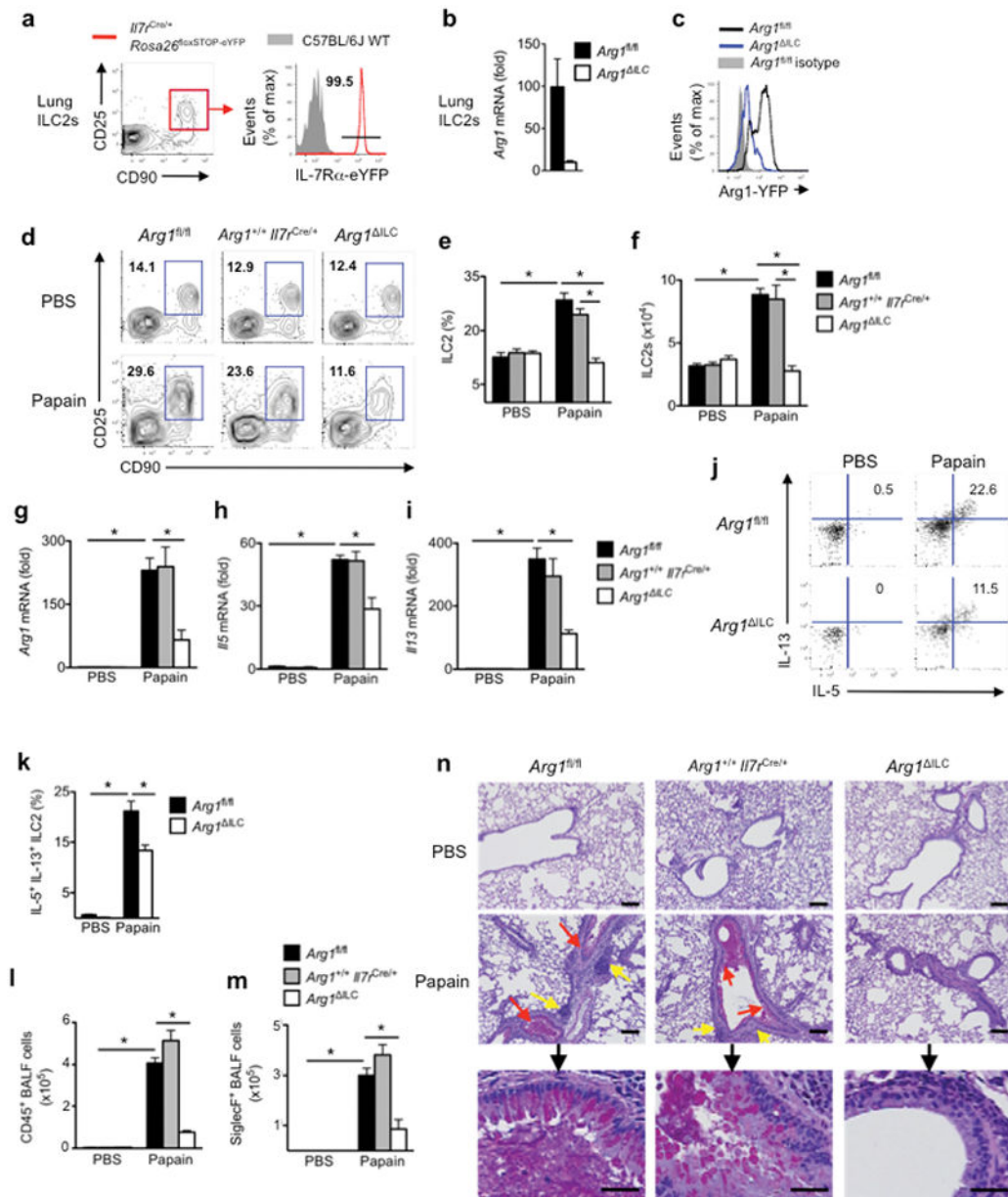
Figure 4. Absence of ILC-intrinsic Arg1 restrains ILC2 responses and dampens airway inflammation

(**a**) Flow cytometric fate-mapping analysis of IL-7Rα expression on lung ILC2s from naive $Il7r^{cre/+}$ $Rosa26^{floxSTOP-eYFP}$ mice or WT mice, pre-gated on Lin⁻ CD45⁺ cells. (**b**) mRNA expression of $Arg1$ in sort-purified lung ILC2s (Lin⁻ CD45⁺CD90⁺CD127⁺CD25⁺IL-33R⁺) from $Arg1^{fl/fl}$ and $Arg1^{ΔILC}$ mice at day 6 of papain treatment, determined by RT-PCR and normalized to β actin levels. (**c**) Representative flow cytometry histogram of intracellular Arg1 expression in naive lung ILC2s (Lin⁻ CD45⁺ CD90⁺ CD25⁺). (**d–n**) $Arg1^{fl/fl}$, $Arg1^{+/+}Il7r^{Cre/+}$, $Arg1^{ΔILC}$ mice were treated with 30 µg papain or PBS i.n. for 5 days and assessed on day 6. (**d**) Representative flow cytometry plots, (**e**) total frequencies, (**f**) cell numbers of lung ILC2s. (**g–i**) mRNA expression of $Arg1, Il5, Il13$ in lung tissue, determined

by RT-PCR and expressed relative to levels in PBS-treated $Arg1^{\text{fl/fl}}$ mice. (**j**) Representative flow cytometric plots and (**k**) quantification of frequencies of lung ILC2s expressing IL-5 and IL-13. ILC2s gated as live, Lin-CD45$^+$CD90$^+$ CD25$^+$IL-33R$^+$. (**l**) Total cell numbers of CD45$^+$ immune cells and (**m**) eosinophils (CD11b$^+$Siglec F$^+$CD11c$^-$) in the bronchoalveolar lavage fluid (BALF) at day 6 post treatment. (**n**) PAS staining of lung sections in PBS or papain-treated mice. Red arrows denote PAS$^+$ goblet cells in the airways, yellow arrows denote foci of immune cell infiltration. Scale bar, 100 μm for large field images, 50 μm for magnified images. All data are representative of three independent experiments with similar results. N = 3 mice per group (PBS) or n = 4 mice per group (papain). Data shown are the mean ± SEM. * p < 0.001 as determined by unpaired Student's *t* test.
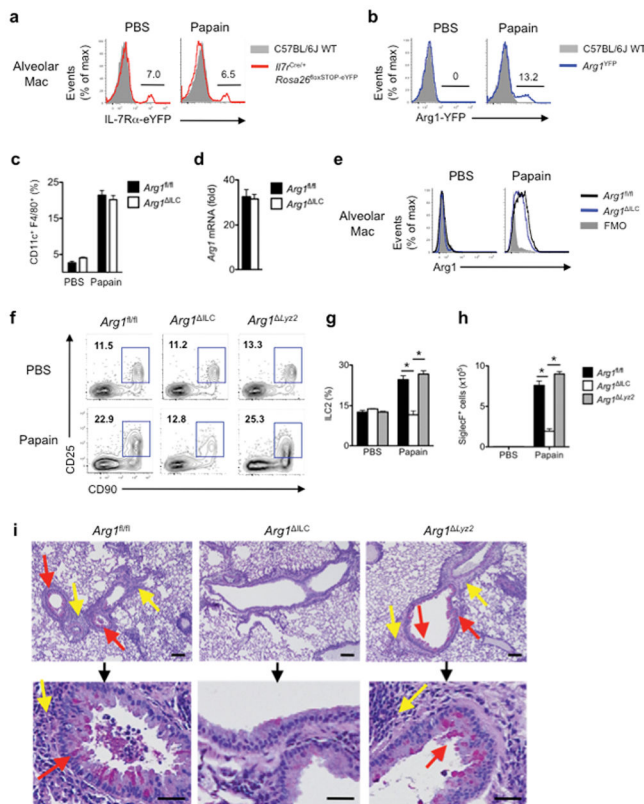
Figure 5. Development of airway inflammation is dependent on ILC-intrinsic, not myeloid cell-intrinsic, expression of Arg1

(**a–b**) Flow cytometric analysis of alveolar macrophages (CD11b⁺CD11c⁺F4/80⁺Ly6G⁻CD3⁻CD19⁻) in (**a**) $Il7r^{cre/+}$ $Rosa26^{floxSTOP-eYFP}$ mice and (**b**) $Arg1^{YFP}$ mice during steady-state and papain-induced airway inflammation at day 6 post-treatment. (**c–e**) $Arg1^{fl/fl}$ and $Arg1^{ΔILC}$ were treated with 30 μg papain or PBS intranasally for 5 days and assessed on day 6. (**c**) total frequencies of lung macrophage (CD11c⁺CD11b⁺F4/80⁺). (**d**) $Arg1$ mRNA expression levels in sort-purified macrophages, normalized to β actin. (**e**) intracellular Arg1 expression in macrophages; FMO (fluorescence minus one), gray shaded. (**f–i**) $Arg1^{fl/fl}$, $Arg1^{ΔILC}$ and $Arg1^{ΔLyz2}$ were treated with 30 μg papain or PBS i.n. for 5 days and assessed on day 6. (**f**) Representative flow cytometry plots and (**g**) total frequencies of lung ILC2s (Lin⁻ CD45⁺CD90⁺CD25⁺). (**h**) Total cell numbers of eosinophils (CD11b⁺Siglec F⁺CD11c⁻) in the BALF. (**i**) PAS staining of lung sections. Red arrows denote PAS⁺ goblet cells in the airways, yellow arrows denote foci of immune cell infiltration. Scale bar, 100 μm for large field images, 50 μm for magnified images. All data are representative of two independent experiments with similar results. N = 2 mice per group (PBS) or n = 3 mice per group (papain). Data shown are the mean ± SEM. * p < 0.001 as determined by unpaired Student's t test.
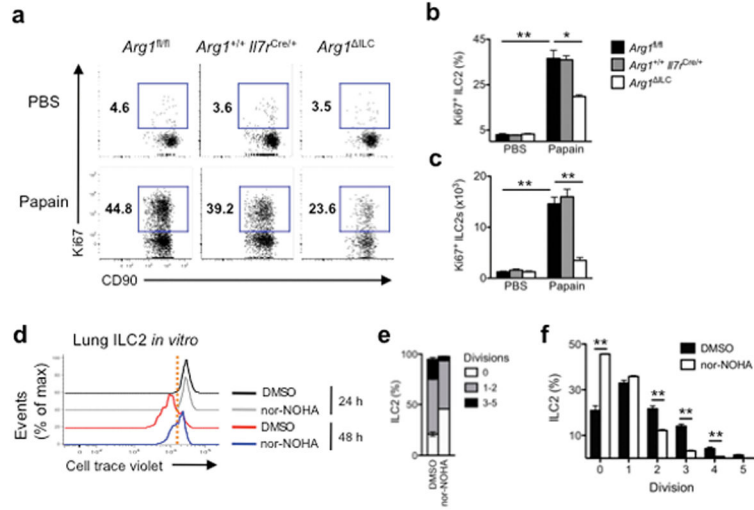
Figure 6. Cell-intrinsic Arg1 controls optimal ILC2 proliferation

(**a–c**) *Arg1*fl/fl, *Arg1*+/+*Il7r*Cre/+, *Arg1* ILC were treated with 30 μg papain or PBS i.n. for 5 days and assessed on day 6 for lung ILC2 proliferation by Ki67 staining. (**a**) Representative flow cytometric plots, (**b**) quantification of Ki67+ ILC2 frequencies (Lin−CD45+CD90+CD25+) and (**c**) total cell numbers. (**d–f**) WT mice were treated with rmIL-33 i.n. and sort-purified lung ILC2s (Lin−CD45+CD90+CD127+CD25+IL-33R+) were labeled with cell trace violet and cultured for 48 h with rmIL-2, rmIL-7, rmIL-33 and DMSO or N$^{\omega}$-hydroxy-nor-Arginine (nor-NOHA). Cells were assessed for dilution of cell trace dye using flow cytometry. (**d**) Representative histogram and (**e,f**) quantification of ILC2 percentage in each cell division. All data are representative of three independent experiments with similar results. N = 3 mice per group. Data shown are the mean ± SEM. *p < 0.01, ** p < 0.001 as determined by unpaired Student's *t* test.
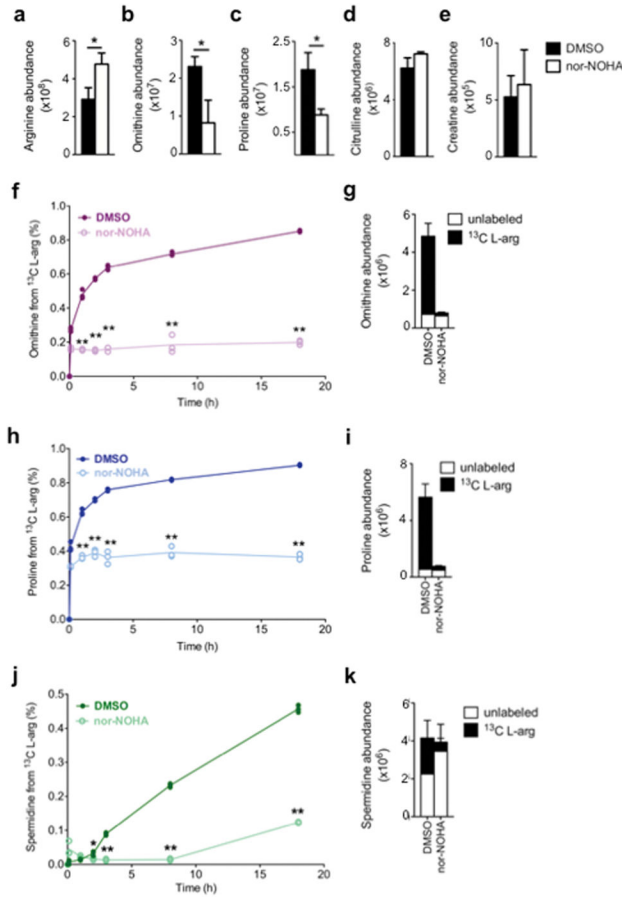
Figure 7. Inhibition of cell-intrinsic Arg1 disrupts balance of amino acid metabolites and impairs polyamine synthesis in ILC2s

(**a–e**) WT mice were treated with rmIL-33 i.n. and sort-purified lung ILC2s were cultured with rmIL-2, rmIL-7 and rmIL-33 in DMSO or nor-NOHA for 24 hrs. Methanol-fixed cells were subjected to liquid chromatography mass spectrometry analysis for levels of (**a**) arginine, (**b**) ornithine, (**c**) proline, (**d**) citrulline, and (**e**) creatine. (**f–k**) WT mice were treated with rmIL-33 i.n. and sort-purified lung ILC2s were cultured with U-^{13}C-L-arginine with rmIL-2, rmIL-7, rmIL-33 and DMSO or nor-NOHA for 18 h. Methanol-fixed cells were subjected to liquid chromatography mass spectrometry isotope tracing analysis to measure incorporation kinetics and relative abundance of the U-^{13}C-L-arginine tracer into (**f,g**) ornithine, (**h,i**) proline, (**j,k**) spermidine. Data are representative of two independent experiments with similar results. N = 3 biological replicates per condition. Data shown are the mean ± S.D. *p < 0.05, ** p < 0.001 determined by unpaired student's *t* test (**a–c**) and two-way ANOVA with Bonferroni post-test correction (**f,h,j**).
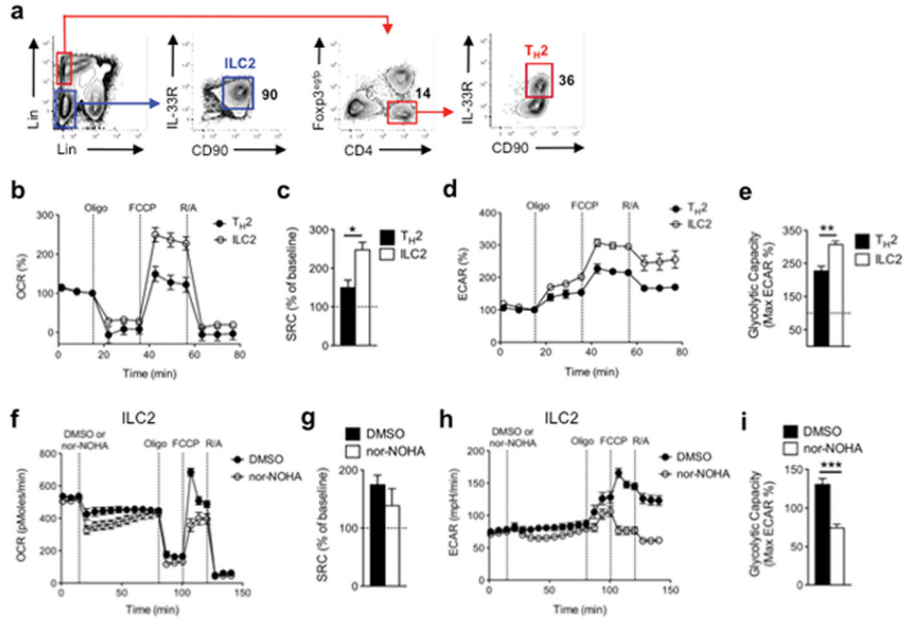
Figure 8. Arg1 controls maximal glycolytic capacity of activated ILC2s
(**a–e**) *Foxp3*^{eGFP} reporter mice were treated with rmIL-33 i.n. ILC2s and T_H2 cells were sort-purified from the lung and assessed for (**b**) OCR (**c**) spare respiratory capacity (SRC, % max OCR after FCCP injection of baseline OCR), (**d**) ECAR, and (**e**) maximal glycolytic capacity (% max ECAR of baseline ECAR) using Seahorse metabolic profiling. (**f–i**) ILC2s were sort-purified from WT mice treated with rmIL-33 i.n. ILC2s were subjected to Seahorse metabolic profiling with DMSO or nor-NOHA injected during measurement of (**f**) OCR, (**g**) SRC, (**h**) ECAR, and (**i**) maximal glycolytic capacity using Seahorse metabolic profiling. (**a–e**) Data shown is combined from two experiments, n = 3 Th2 cell replicates and 12 ILC2 replicates. (**f,h**) Data shown are from one representative experiment out of 4 experiments with similar results, n = 7 DMSO replicates and 7 nor-NOHA replicates. (**g,i**) Data shown is combined from 4 experiments, n = 18 DMSO replicates and 16 nor-NOHA replicates. (**b–i**) Data shown are the mean ± SEM. * $p < 0.05$, **$p < 0.01$, *** $p < 0.001$, as determined by unpaired Student's *t* test.